Tissue Regeneration in the Shell of the Giant Queen Conch, *Strombus gigas*

Xiao-Wei Su,*,† Dong-Mei Zhang,† and A. H. Heuer*

Department of Materials Science and Engineering, Case Western Reserve University, Cleveland, Ohio 44106

Received July 17, 2003. Revised Manuscript Received November 12, 2003

The crossed-lamellar microarchitecture (microstructure) of the shell of *Strombus gigas*, the giant Queen conch native to Caribbean habitats, is the most common of the several shell microarchitectures known in the mollusk family. We have studied tissue regeneration in juvenile *S. gigas* conchs and compared the microstructure in this regenerated tissue to the microstructure of wild *S. gigas* shells. The regenerated hard tissue was of two types: hard tissue grown during wound repair, and so-called "flat pearls" which are hard tissue grown on abiotic substrates inserted between the mantle and the outer covering. In both cases, the crossed-lamellar microstructure is observed after formation of a transition structure consisting of a large quantity of matrix and aggregates of aragonite crystallites.

I. Introduction

The microstructures of mollusk shells are of interest on several counts. These shells are among the most heavily mineralized of hard tissue, and understanding of their growth and repair is an important issue in current biomineralization research. Second, these shells can be considered high-performance laminated biocomposites, with their impressive mechanical properties arising from the particular arrangements of the constituent $CaCO_3$ biominerals and the organic "matrix" (the nonmineral portion of mineralized tissue, which contains proteins, carbohydrates, polysaccharides, and "structural" water).[1] Thus, microstructure/mechanical property correlations are important for materials engineers attempting to design new composite structures "biomimetically".

The crossed-lamellar microarchitecture is the most common of the several shell structures known in the mollusk family,[2,3] and the fracture toughness of shells with this microarchitecture is significantly greater than that of shells with other microarchitctures.[4,5] The volume fraction of organic matrix in shells with the crossed-lamellar microstructure is very small (≤2%) and comparable to that of tooth enamel which is the most highly mineralized of all mammalian hard tissue.[6]

There are five different length scales that characterize the structure of the crossed-lamellar microarchitecture in *Strombus gigas*, the giant Queen conch native to Caribbean habitats: macroscopic layers; first order, second order, and third-order lamellae within each layer; and fine scale twins within the third-order lamellae.[4] Like most gastropods with the crossed-lamellar structure, the $CaCO_3$ is aragonitic in *S. gigas*.[1,2]

During growth of *S. gigas*, shell development takes place at the outer lip of the aperture or shell opening,[7] which extends at a rate of 0.3 to 0.6 mm/day. (The growth rate varies with the age of the animals and the environment where the animals live.[8]) The outer mantle epithelium, the "skin" or membrane covering the soft body parts of the animal, controls the deposition of the shell.[9] It delivers both the mineral-forming and organic components into the extrapallial fluid lying between the mantle epithelium and the shell. The growth of the shell is preceded by development of the periostracum, an organic membrane on the outer surface of the shell that protects the shell and provides a base on which the inner shell layers are deposited.[10] During biomineralization, the periostracum increases in thickness; this is followed by deposition of additional organic substance on the inner surface. Eventually, crystalline aragonite nucleates and grows on the periostracum.

Although the shells in mollusks are essentially inert, unlike mammalian bone for example, they are key to their defenses against predators. Mollusks are capable of repairing damage inflicted to the shell, with the repair being accomplished by deposition of new shell material in the damaged area. Crystal deposition and the formation of the organic matrix of shell are also controlled by

* To whom correspondence should be addressed. Fax: 216-368-8932. E-mail: sux@bme.ri.ccf.org; heuer@case.edu.

† Now at the Lerner Research Institute/ND20, The Cleveland Clinic Foundation, 9500 Euclid Ave., Cleveland, OH 44115.

(1) Lowenstam, H. A.; Weiner, S. *On Biomineralization*; Oxford University Press: New York, 1989.

(2) Currey, J. D. In *Skeletal Biomineralization: Patterns, Processes and Evolutionary Trends*; Carter, J. G., Ed; Van Nostrand Reinhold: New York, 1990; pp 11−25.

(3) Bøggild, O. B. *K. Danske Vidensk. Selsk. Skr.* **1930**, *2*, 232.

(4) Kuhn-Spearing, L. T.; Kessler, H.; Kessler, S. M.; Ballarini R.; Heuer, A. H. *J. Mater. Sci.* **1996**, *31*, 6583.

(5) Jackson, A. P.; Vincent, J. F. V.; Turner, R. M. *Proc. R. Soc. London* **1988**, *B234*, 415.

(6) Osborn, J. W.; Grly, P.; Silverstone, L. M. *Dental Enamel; Development, Structure and Caries*; Munksgaard: Copenhagen, 1973.

(7) Vermeil, G. J. In *Skeletal Growth of Aquatic Organisms*; Rhoads, D. C., Lutz, R. A., Eds; Plenum Press: New York, 1980; pp 379−389.

(8) Ray, M.; Stoner, A. W. *Mar. Ecol. Prog. Ser.* **1995**, *123*, 82.

(9) Wilbur, K. M. In *Chemical Zoology*; Florkin, M., Scheer, B. T., Eds; Academic Press: New York, 1972; pp 103−145.

(10) Nakahara, H.; Kakei, M.; Bevelander, G. *Veliger* **1981**, *23*, 207.

10.1021/cm030573l CCC: $27.50
Published on Web 01/21/2004

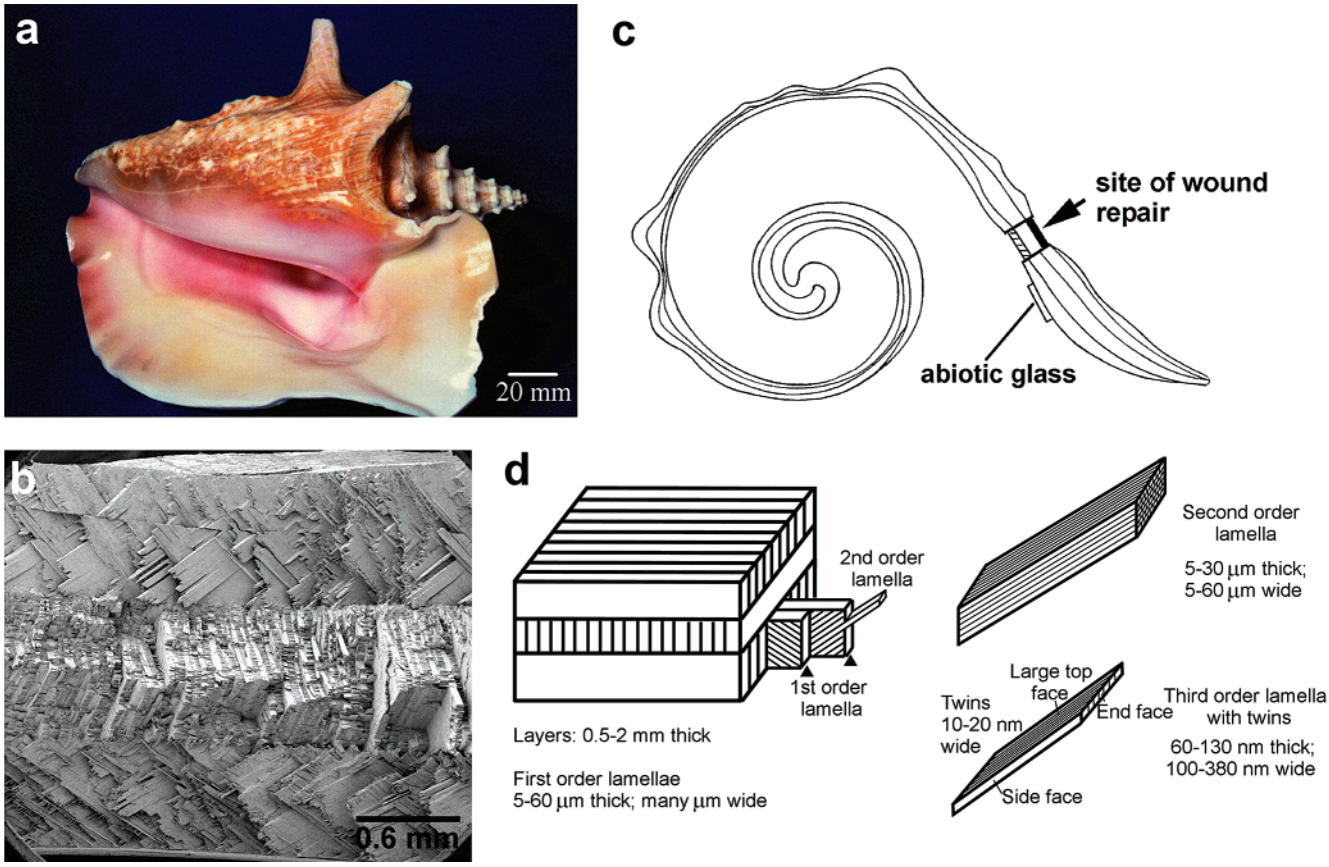

Figure 1. (a) Shell of a wild conch, *S. gigas*. (b) Low magnification SEM image of fractured shell. The bend specimen was taken from the last whorl. (c) Schematic drawing showing the shell cross section. (d) Schematic drawing of the crossed-lamellar microarchitecture.

mantle tissue.[11] In this regard, shell regeneration has many similarities to shell formation.[9,11]

There have been several studies of shell regeneration in the past, but for gastropods, almost all studies were confined to species of *Helix*.[12,13] Different species respond to damage in different ways. The repaired tissue may be similar to the original hard tissue or may be different in the chemistry of organic matrix and/or in the polymorph of minerals.[11] It is generally accepted that when repair takes place at the shell edge, the structure of the repaired shell is essentially the same as that for wild shells. If the damage occurs away from the shell edges where the mantle cannot retract, the repaired shell is often different from the normal shell in its structure, the composition of the organic matrix, and the mineralogy and morphology of the crystalline phases.

Hard tissue regeneration in *S. gigas* has not received much attention in the past, but can be studied in convenient times using juvenile animals; the shell of this organism provides us with an excellent model system for studying biomineralization in invertebrates.

Though the structure of crossed-lamellar shells has been studied for many years, previous microstructural studies have not satisfactorily resolved the structural details of matrix/mineral interfaces at each length scale in this very heavily mineralized shell. During this work, we have studied wild shells in detail, and in this paper we present a detailed microstructural analysis of wild and regenerated shell of *S. gigas*. Microstructures have been characterized by scanning and transmission electron microscopy (SEM and TEM, respectively) and high-resolution electron microscopy (HREM), and these studies have been augmented by X-ray diffraction (XRD) analysis. We further characterize the crystallographic texture of the aragonite crystals and the distribution of organic matrix. A brief description of some of this work has been published elsewhere.[14]

II. Experimental Procedure

Juvenile *S. gigas* conchs were obtained from the Caribbean Marine Research Institute (Jupiter, FL), whereas wild shells were obtained from a commercial source (Holiday Souvenir, Ft. Lauderdale, FL. Shells were supplied without undergoing the usual treatment (cleaning, bleaching, etc.) to which such shells are subjected prior sale to the public.) To study the microstructure of wild conch shell by SEM, both fractured samples and polished and partially demineralized samples were used. Fractured samples were obtained using four-point bending experiments.[4] Partially demineralized samples were prepared by the following procedure. Shell pieces were sectioned with a Buehler Isomet 11-1180 low speed saw (Lake Bluff, IL) fitted with a diamond blade. The sides of the specimens were polished using 600, 1200, and 2400 grit SiC paper, followed by 3-μm diamond abrasive. The polished surfaces of the specimens was partially demineralized by

(11) Watabe, N. In *Shell Repair in The Mollusca*; Saleuddin, A. S. M., Wilbur, K. M., Eds; Academic Press: New York, 1983; Vol. 4 Physiology, Part 1, pp 289−316.
(12) Saleuddin, A. S. M.; Chan, W. *Can. J. Zool.* **1969**, *47*, 1107.
(13) Saleuddin, A. S. M.; Wilbur, K. M. *Can. J. Zool.* **1969**, *47*, 51.
(14) Kamat, S.; Su, X.; Ballarini, R.; Heuer, A. H. *Nature* **2000**, *405*, 1036.

immersing the shell in 5% ethylenadiaminetetracetic acid (EDTA, a calcium ion chelator) for 7 days with a change of EDTA solution every day. Samples were then coated with gold and observed in a Hitachi-S4500 FEG SEM (San Jose, CA) operating at 2 kV. Petrographic thin sections of wild shell, about 30 μm thick, were prepared in three different orientations parallel to the three major faces of the third-order lamellae (Figure 1d): the "large" top face, the small "end" face, and the "side" face. These were then thinned using a Gatan model 600 ion beam thinner (Warrendale, PA) until they were electron transparent and were examined at either 200 keV accelerating voltage in a Philips CM20 conventional TEM (Mahwah, NJ) or at 400 keV in a JEOL 4000 EX HREM (Peabody, MA). In some cases, it was desired to study isolated third-order lamellae. These were prepared by grinding a shell into powder under ethanol using an agate mortar and pestle and dispersing a drop of the supernatant slurry onto a copper grid such that the crystallites were oriented with their large top faces normal to the electron beam.

To induce shell regeneration, one of two techniques was used. In the first—wound repair—a 4-mm diam hole was cut in the shell with an electric drill about 40 mm away from the shell edges (Figure 1c). (To avoid injury of the mantle tissue, we stimulated the animals manually to make the mantle withdraw beyond the shell area that was to be drilled.) In some cases the hole was covered with a thin (0.2 mm) polystyrene cap, while in other cases the hole was left uncovered. The animals were then returned to a research-grade aquarium (West Coast Aquatics, Thousand Oaks, CA) and left for up to 10 days. The saltwater temperature was maintained between 20 and 26 °C. During this period, food was given twice a day. At intervals of 1, 2, 4, 6, 8, and 10 days, the regenerated portion of the shell was removed with a forceps, rinsed with distilled water and dried in air. In the second shell regeneration technique, conch "flat pearls" were grown by inserting abiotic substrates (glass cover slides in the work reported here) between the mantle tissue of the animal and the inner layer of the shell (Figure 1c).

Cross-sectional SEM samples of regenerated shell were prepared by gluing two pieces of shell together using an epoxy adhesive, polishing a flat surface using 1200 grit SiC paper followed by 3-μm diamond abrasive on a Buehler polishing wheel (Lake Bluff, IL), and briefly etching for 1 min with EDTA. Plan-view TEM samples were prepared by one-sided ion-thinning using a single gun incident on the side away from the glass substrates. Cross-sectional TEM samples were prepared from the same type of sample used for SEM analysis, again employing standard ion thinning techniques.

XRD (Scintag X-1 system San Jose, CA, Cu Kα radiation at 40 kVa,) was employed to identify the crystal structure and possible texture of regenerated shell. Both the inner layer of a wild shell and shell powder (prepared by crushing and grinding a small piece of shell in a mortar and pestle) were used as controls.

III. Results and Discussion

3.1 Structure of Wild *S. gigas* Conch Shells. Figure 1a shows a mature wild shell, and Figure 1b shows a fractured surface of a bend specimen prepared from such a shell in which the 3 layers of the shell are immediately obvious. The bulk of the shell has only these 3 layers, termed inner, middle, and outer for obvious reasons. Growing whorls can occasionally have more than three layers, as is suggested by the schematic drawing of the shell cross-section shown in Figure 1c.

The hierarchical structure of each layer is identical and is shown schematically in Figure 1d, which also includes data on characteristic dimensions of each of the components of the layers. The details of Figure 1d will become clear from the SEM and TEM data to be presented below (Figures 3−5 and 9b). In terms of the basic structure, however, all layers have the identical structure but are rotated by ~90° from their immediate neighbors.

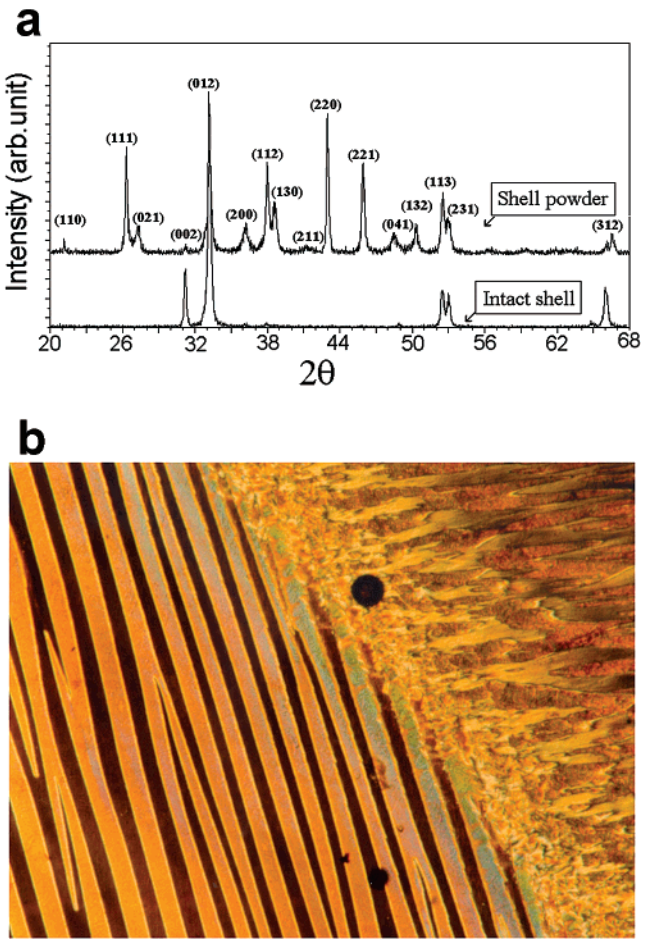

Figure 2. (a) XRD patterns of intact shell and of ground-up shell powder. (b) Optical micrograph (petrographic thin section between crossed polars) showing the interface between the inner (on the left) and middle (on the right) layers. The first order lamellae in the inner layer are clearly visible. Alternate first-order lamellae go extinct on rotation between fixed crossed polars every 90°. The width of the image is approximately 0.5 mm.

Figure 2a shows XRD patterns obtained from shell powder and from the inner surface of a shell fragment. The intensity and *d* spacings of the labeled peaks of the shell powder pattern correspond to the 2θ angles of XRD peaks of abiogenic aragonite, as listed in the JCPDS card file (Swarthmore PA, card 5-0453). The pattern of the intact shell shows a distinct texture; the intensities of the (002) and (012) reflections are much stronger than that for a random orientation, and the intensities of the (110), (111), (021), (200), (112), (130), (220), (221), (041), and (132) peaks are essentially zero.

Study of petrographic thin sections between crossed polarizers in an optical microscope equipped with a rotating stage revealed that the first-order lamellae within each layer went into optical extinction as a single unit for every 90° rotation of the stage (Figure 2b); this is further evidence of a strong crystallographic texture. The TEM data to be discussed next will provide further details of the nature of the growth texture of this highly structured hard tissue.

The basic building blocks of the crossed-lamellar microarchitecture were identified as third-order lamel-

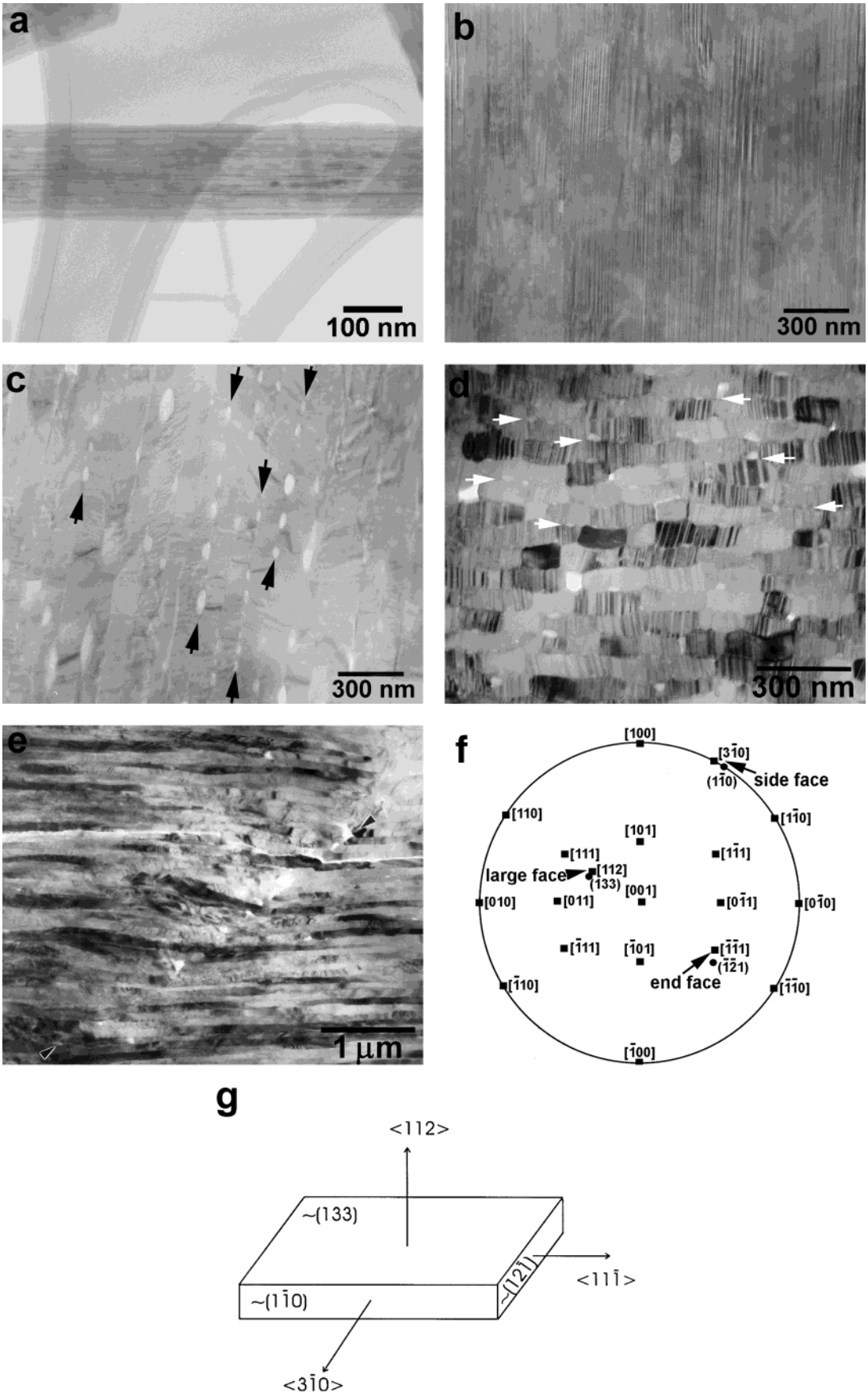

Figure 3. TEM images: (a) an isolated third order lamellae; (b−d) images taken normal to the large face (b), the side face (c), and the end face (d); (e) third-order lamellae are not continuous throughout a second-order lamellae. (f) Sterographic projection of aragonite centered on [001]; only a few plane normals are included (see text for further discussion). (g) Schematic drawing of an isolated third-order lamella, showing the approximate orientation of the basic building block of the shell.

lae in previous studies.[4,14] A TEM micrograph of an isolated rectangular third-order lamella is shown in Figure 3a. As already noted, thin sections parallel to the three faces of rectangular third-order lamellae have been prepared to study the detailed organization of these lamellae into second-order lamellae and the organization of second-order lamellae into first-order lamellae. TEM images were taken in various orientations such that the electron beam was normal to either the large faces (Figure 3b), the side faces (Figure 3c), or the end faces (Figure 3d). The end-face images are the most instructive.

The organization of third-order lamellae into a second-order lamella is akin to that of a brick and mortar structure. The lamellae are stacked in layers, and within any one layer, the large faces of third-order lamellae are well aligned. The interfaces between side faces from the top to the bottom layer of the third-order lamellae form a zigzag path. The long axes of the third-order lamellae are approximately parallel to one another. The fact that the third-order lamellae are not all in strong diffracting conditions at the same time at a given orientation of the TEM foil in Figure 3d is good evidence that the third-order lamellae are not in perfect crystallographic registry.

The width and thickness of third-order lamellae can be measured using images similar to those in Figure 3. The widths range from 140 to 300 nm, with an average width of 220 nm, and the thicknesses range from 65 to 125 nm, with an average thickness of 95 nm. The length is somewhat difficult to determine with TEM because the third-order lamellae are extremely long and the electron transparent area is limited. We estimated that the lamellae are several micrometers long. In this regard, Figure 3e shows that the third-order lamellae are not continuous throughout the thickness of a macroscopic layer; the arrowed feature in Figure 3e shows a boundary where 2 third-order lamellae abut one another.

As is apparent from Figure 3d, the large top faces and side faces of the third-order lamellae are not well-defined crystallographically. However, the approximate orientation of the three faces can be determined using the oriented thin foils referred to earlier, as well as the orientation of isolated third-order lamellae.

Isolated crystallites (Figure 3a) were used for large-face diffraction studies. Microdiffraction patterns were taken from the separated crystallites. Without tilting, 12 microdiffraction patterns were taken from large top faces: 10 showed a ⟨112⟩ zone axis, one showed a ⟨111⟩ zone axis, and one showed a ⟨221⟩ zone axis.

Samples for side-face diffraction were chosen from among conventionally prepared TEM foils by selecting third-order lamellae whose long axes were parallel to the sample (i.e., we required that the whole length of the third-order lamellae be visible within the electron transparent area and that the proteins between large faces be clearly resolved). Microdiffraction zone axis patterns were then taken after tilting to the closest zone axis, with tilting being restricted to small angles (within ±7°). Among the 20 diffraction patterns taken from side faces, seventeen showed a $\langle 3\bar{1}0\rangle$ zone axis, one showed a $\langle 9\bar{3}2\rangle$ zone axis, one showed a $\langle 1\bar{3}2\rangle$ zone axis, and one showed a $\langle 4\bar{2}1\rangle$ zone axis. Thus ⟨112⟩ and $\langle 3\bar{1}0\rangle$ are taken as the nominal plane normal orientations for large and side faces, respectively.

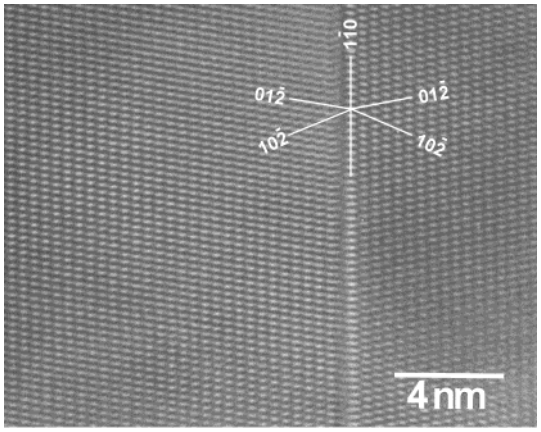

Figure 4. HREM image of a $(1\bar{1}0)$ twin boundary in a third-order lamella ($[\bar{2}\bar{2}1]$ zone axis).

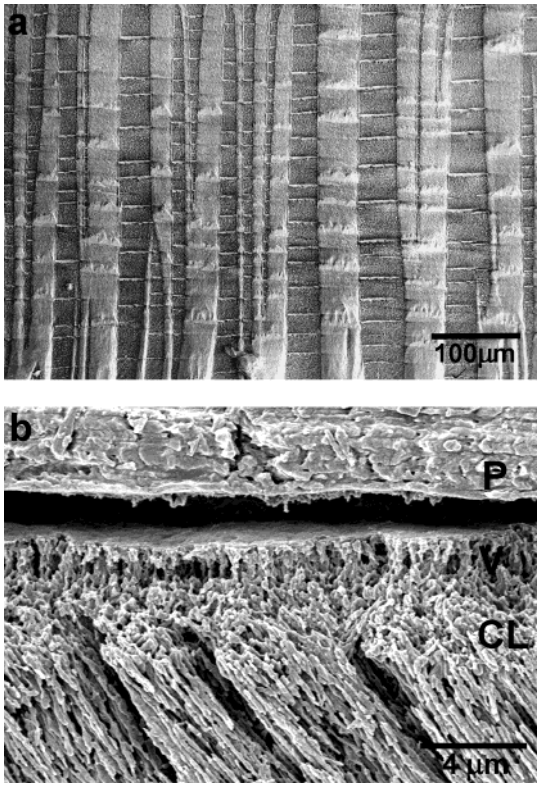

Figure 5. (a) and (b) SEM micrographs of partially demineralized polished sections. The contrast in (a) reveals the organic matrix "interphase" separating first- and second-order lamellae; the second-order lamellar interfaces are the bright horizontal features. (b) The periostracum (P), a thin layer of vertically oriented crystallites (V), which are the first minerals to form, and the crossed-lamellar microarchitecture itself (CL). The gap between the periostracum and the layer of vertical crystals occurred during drying of the shell.

To decide the orientation of the end faces is more difficult. We determined this orientation stereographically as follows. First, a [001] stereographic projection was drawn and the $\langle 3\bar{1}0\rangle$ side-face zone axis orientation was noted (Figure 3f). As the individual third-order lamellae can be approximated by rectangular parallelopipeds, the other two plane normals must be perpendicular to $\langle 3\bar{1}0\rangle$ and be on a great circle 90° away from this zone. The large-face plane normal orientation,

⟨112⟩, is in fact very close to this great circle, and 90° from ⟨112⟩ on this great circle yields the end-face plane normal orientation, ⟨11$\bar{1}$⟩. The approximate crystallographic orientation of the three faces is shown schematically in Figure 3g.

Extensive twinning can be seen in the end- and large-face orientations, but not on the side-face orientation. The near vertical stripes in each third-order lamella in Figure 3d are individual twins, with the twin plane being approximately parallel to the side faces of third-order lamellae, parallel to the (1$\bar{1}$0) plane. The twin traces reveal that misorientation between adjacent third-order lamellae varies between 10° and 20°.

Figure 4 is a HREM image of a twin boundary observed with the beam direction parallel to [$\bar{2}\bar{2}$1]. The twin boundary is atomically flat and defect-free. No dislocations or other crystallographic defects have been observed using HREM.

Whereas twinning occurs on both and (110) and (1$\bar{1}$0) planes in geological aragonite,[15] biogenic aragonite in nacre,[16] and the molluskan hinge ligament,[17] twinning occurs exclusively on (1$\bar{1}$0) planes in the crossed-lamellar structure in conch shells (twinning on the crystallographically equivalent (110) plane does not occur). The difference between twinning in nacreous aragonite and that in the crossed-lamellar structure is related to morphological differences of the individual crystallites.[16] Given that the twin boundaries are dislocation-free and that the aragonite is grown at ambient temperature, it is clear that the twins are not deformation twins nor annealing twins but growth twins. We suggest that the high density of twin boundaries develop from growth accidents during rapid shell formation (as already noted, growth rates of 0.3−0.6 mm/day have been reported[8]).

We turn now to the organic matrix, which is intimately associated with the third-order lamellae. The globular features (shown by arrows in Figure 3c and d) are the most visible evidence of such organic matter. They are clearly visible distributed between the large faces of the third-order lamellae, but are difficult to resolve between the side faces (Figure 3b and d).

Besides the organic matrix associated with the third-order lamellae, matrix is also present along first-order and second-order lamellar interfaces and can be seen most readily in SEM images of partially demineralized polished sections (Figure 5a). The first- and second-order lamellar interfaces are clearly resolved in this figure. Copious organic matrix exists at the interfaces between second-order lamellae within individual first-order lamella, i.e., the interfaces between second-order lamellae are thicker than the interfaces separating first-order lamellae.

The other important matrix component is the external periostracum. This can be seen in Figure 5b, also from a partially demineralized section. (The periostracum has pulled away from the mineralized part of the shell in this image.) A thin (∼2 μm) layer of vertically oriented

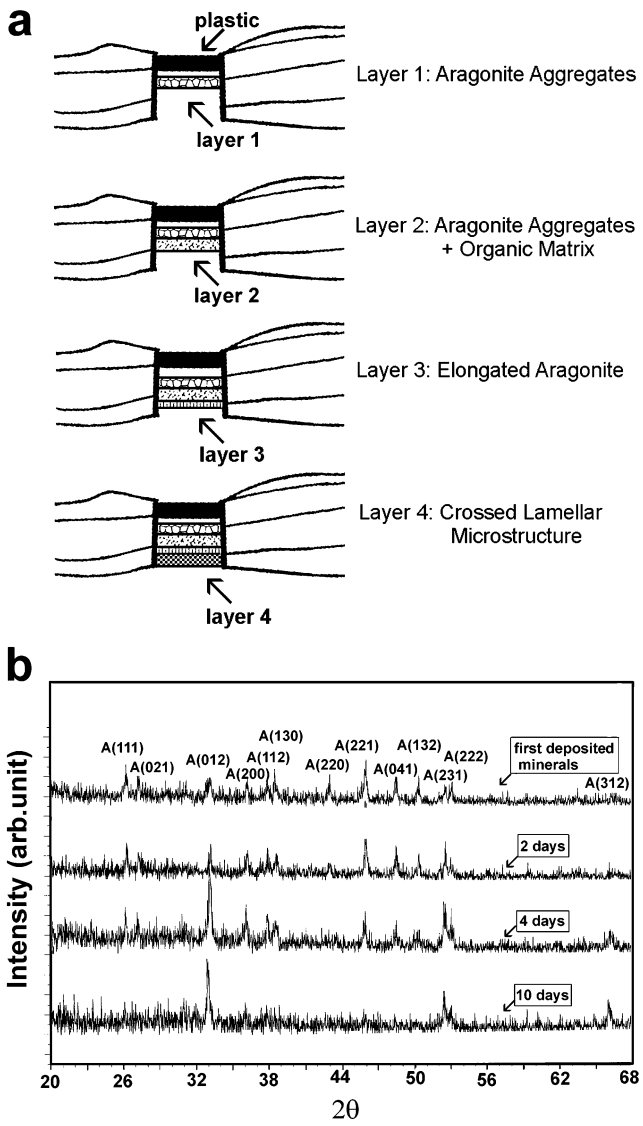

Figure 6. (a) Series of schematic drawings detailing the regeneration process during wound repair; (b) XRD patterns of regenerated tissue at various times of the wound repair process.

crystallites abuts the periostracum. These are the first minerals formed during development of the shell; the crossed-lamellar structure forms on this vertical layer.

It is clear that the heavily mineralized shells in conchs have evolved to protect the animals from attack by predators. The inner surface of the shell will be under tension when attacks occur, with the third-order and second-order interfaces being at an angle of ∼45° to the inner surface of the shell. First-order interfaces are perpendicular to the inner shell surface. Thus, first-order interfaces are the "weakest" interfaces, and "channel cracks" form along first-order interfaces during loading, as has been noted in other work from our group.[4] As the first-order interfaces change by 90° from their orientation in the inner macroscopic shell layer to that in the middle macroscopic layer, channel cracks will be arrested when approaching an inner layer/middle layer boundary. As the boundary is not planar but zigzags, channel cracks must propagate approximately 45° to the original crack direction to enter second-order and third-order interfaces. Clearly, the high density of second- and third-order interfaces are

(15) Wenk, H. R.; Barber, D. J.; Reeder, R. J. In *Reviews in Mineralogy*; Reeder, R. J., Ed.; Mineralogical Society of America: Washington, DC, 1983; Vol. 11, pp 301−367.

(16) Sarikaya, M.; Aksay, I. A. In *Structure, Cellular Synthesis and Assembly of Biopolymers*; Case, T., Ed.; Springer-Verlag: Berlin, 1992; pp 10−26.

(17) Marsh, M. E.; Sass, R. L. *Science* **1980**, *208*, 1262.

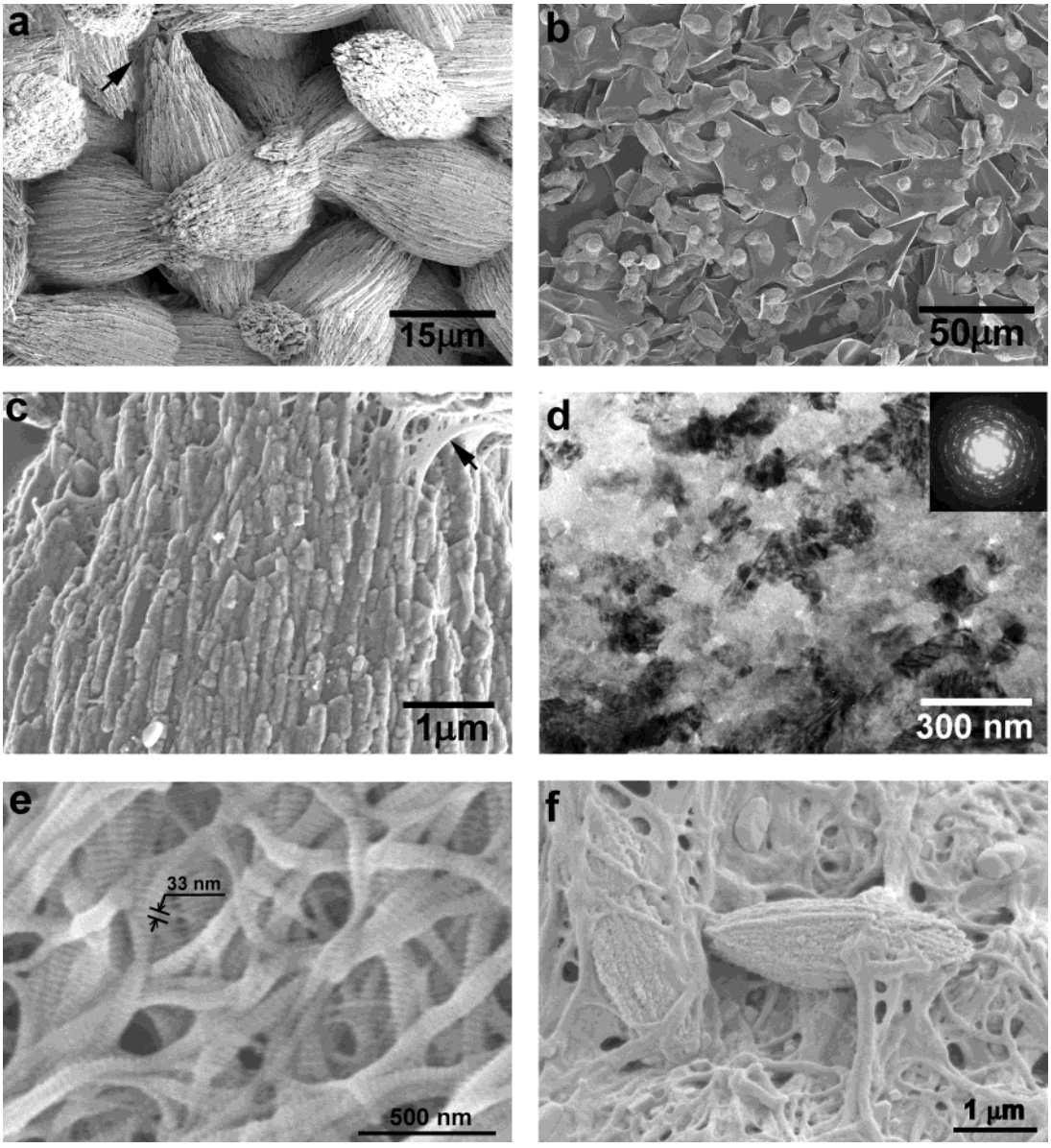

Figure 7. (a) Aragonite aggregates on lid side of membrane, corresponding to layer 1 of Figure 6a. (b) and (c) Similar aggregates embedded in organic matrix on the mantle side of the membrane. (d) TEM micrograph of the aggregate of aragonite crystallites. (e) and (f) A collagenous matrix that forms when wound repair occurs without a lid (the 33-nm banded structure characteristic of collagen is indicated in (e)).

beneficial to the energy dissipation associated with the multitude of microcracks, as well as the crack bifurcation that occurs during catastrophic failure of the shell. Thus, the equisite crossed-lamellar microstructure contributes in a major way to the very large overall work of fracture and exceptional fracture toughness of mollusk shells compared with conventional brittle ceramics or mineral aragonite (see Figure 10 of Kuhn-Spearing et al.[4]). Because the second-order lamellar interfaces in alternate first-order lamellae in the middle layer are oriented roughly 90° to each other, cracks propagating along second-order interfaces in an individual first-order lamella cannot penetrate through to their neighboring first-order lamellae. Crack bridging occurs and results in the marked "orientation" toughening of the crossed-lamellar microarchitecture.

3.2 Microstructure of Regenerated Shell of *S. gigas* Formed during Wound Repair. Figure 6a shows a schematic diagram of the wound repair process. The plastic "lid" served mainly to limit the loss of nutrients that are secreted by the mantle tissue for use during wound repair. Formation of the organic matrix and associated minerals starts immediately after injury. Shell repair was initiated by the deposition of sheets of organic matrix and aggregates of crystallites (layer 1 in Figure 6a). It takes up to 24 h for the damaged area to be completely covered by regenerated tissue, but as we now will show, it takes up to 8 days to form the crossed-lamellar microstructure characteristic of wild shells.

XRD patterns of the regenerated shell material are shown in Figure 6b. The first deposited material is randomly oriented aragonite, the same polymorph of $CaCO_3$ as in wild shell. The preferred orientation (the crystallographic texture) characteristic of the crossed-lamellar microarchitecture takes longer to develop (at least a week), but can clearly be seen in the data from the 10-day sample shown in Figure 6b.

We will now present images of the regenerated tissue grown with and without the lid shown in Figure 6; the "lid" data will be presented first. The first matrix material to appear at the site of the wound is a transparent, colorless, fibrillar membrane, formed within ~24 h after injury, a few hundred nm in thickness. The surface of the organic membrane is optically smooth.

Within 48 h, spindle-shaped aggregates of crystallites are deposited on the membrane and render the membrane optically opaque. Similar aggregates have been observed in regenerated shell of other mollusks. The aggregates on the lid side of the membrane (layer 1 in Figure 6a) are shown in Figure 7a; they completely cover the membrane. The aggregates shown in Figure 7a are 5−10 μm long and 3−5 μm thick and appear to contain needlelike crystallites ("needlelike" crystallites are the usual morphology for nonbiogenic aragonite.) Between the aggregates, a few sheets of organic matrix can be seen (shown by arrow in Figure 7a).

A mantle-side view of the regenerated tissue, showing aggregates of crystallites embedded in the membrane, is shown in Figure 7b; this region corresponds to layer 2 in Figure 6a. A higher magnification image of one of the "inside" aggregates is shown in Figure 7c. The minerals are polycrystalline and consist of many needlelike crystallites; the close association of the mineral phase with the fibrillar membrane is apparent (region shown by arrow in Figure 7c). The diameters of the fine fibers that form the organic membrane vary from 30 to 60 nm.

Figure 7d is a TEM image taken from a plan view foil of the initially formed regenerated material. The regenerated material contains fine crystallites, ~50 to ~100 nm thick, some of which are twinned on a fine scale; the twinning is almost certainly a result of rapid crystal formation.

Figure 7e and f show organic matrix deposited during wound repair when the lid is absent. The first formed material is collagenous (Figure 7e); curiously, collagen was not present when wound repair took place in the presence of a lid. The initially formed mineral in the lidless wound repair is also aggregates of needlelike aragonite (Figure 7f), after which the microstructural development is similar to that which occurs when the lid is present.

Further growth of the regenerated shell resulted in the deposition of elongated minerals (layer 3 of Figure 6a) perpendicular to the growing surface of the regenerated shell. Figure 8 shows an end-on view of such elongated crystals. (Longitudinal view of this structure is shown at the upper part of Figure 10d). We believe that this morphology is comparable to the elongated crystals adjacent to the periostracum shown in Figure 5b. Fiberlike matrix is also present between crystallites (arrowed in the figure). As in wild shell, such perpendicularly oriented elongated crystals precede the deposition of the crossed-lamellar structure (layer 4 of Figure 6a).

As noted already, the crossed-lamellar structure forms within 8 days of initiation of shell repair. Figure 9a shows an SEM micrograph of the inner surface of 10-day regenerated shell tissue. For comparison, the inner surface of a wild conch shell is shown in Figure 9b. Although the crossed-lamellar structure is indeed formed during wound repair, it is not as well organized as that present in wild shell.

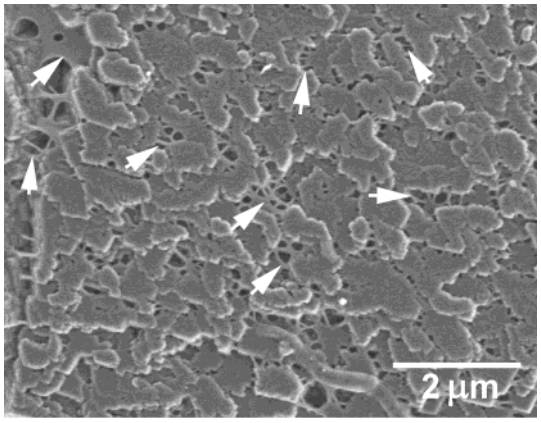

Figure 8. SEM image ("end-on" view) of elongated crystals corresponding to layer 3 of Figure 6a.

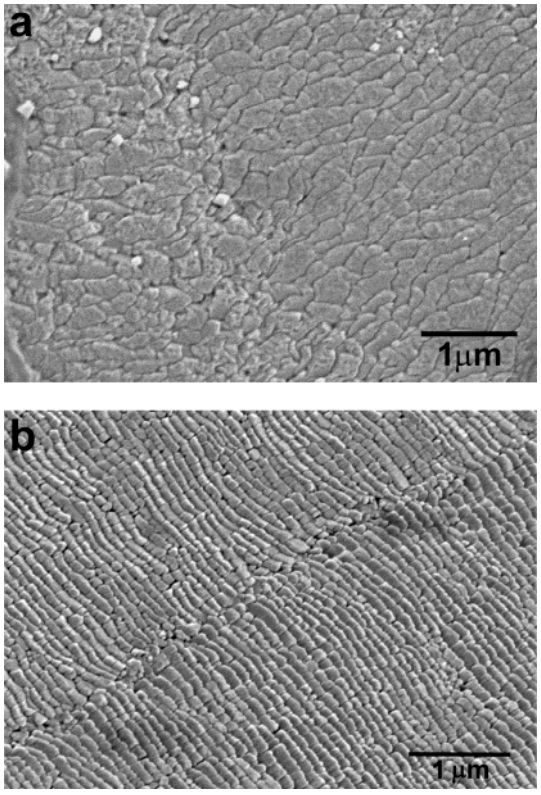

Figure 9. (a) SEM image (inside view) of fully developed crossed-lamellar microstructure formed after 10 days of wound repair. The morphological "texture" of the inside of the wild shell is shown in (b). Characteristic of the crossed-lamellar microarchitecture in wild shell (b) is more well developed than in the regenerated tissue (a).

The regenerated tissue was also studied using cross-sectional samples in the SEM (Figure 10). About 100 micrometers of abnormal tissue had formed before the deposition of the "normal" crossed-lamellar shell structure, as is shown in Figure 10a−c. A large quantity of laminated organic sheets and aggregates of crystallites deposited on the organic sheets are further aspects of the "abnormal" structure which is not present in wild conch shell. The layer of elongated crystals perpendicular to the shells, which precedes the formation of the crossed-lamellar structure, is shown in Figure 10d.

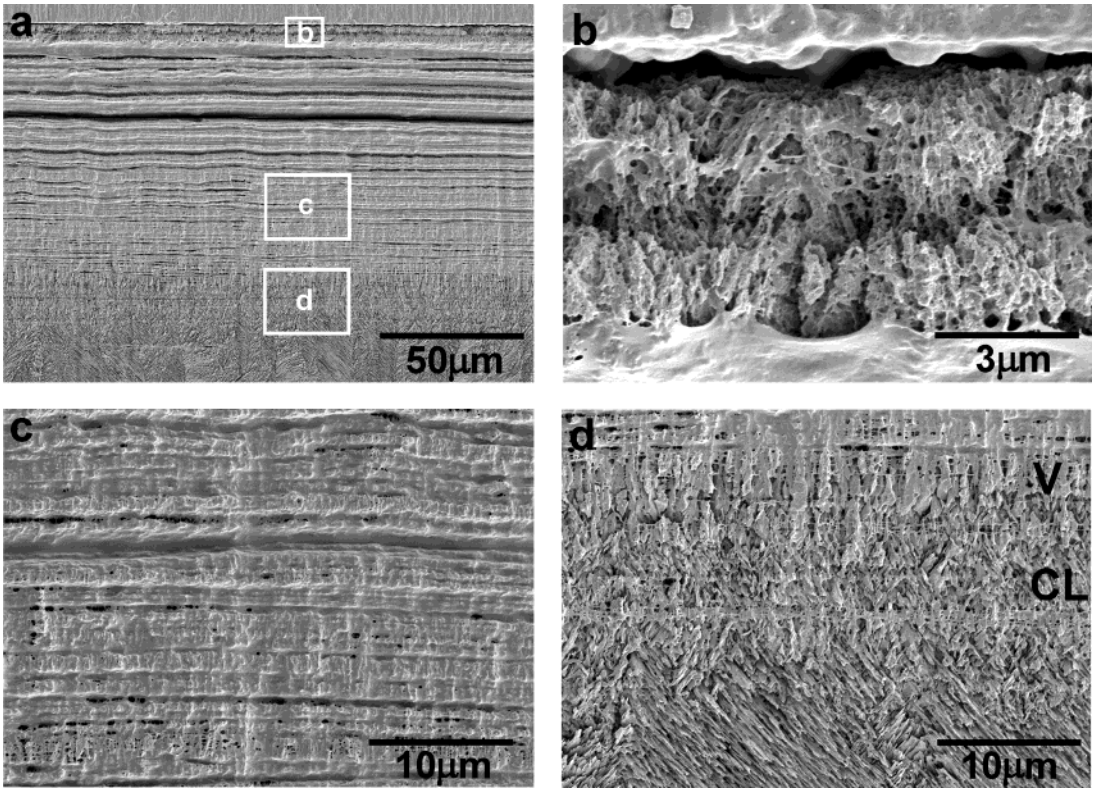

Figure 10. Cross-sectional SEM images of regenerated tissue developed during wound repair: (a) shows that ~100 μm of hard tissue must form before the crossed-lamellar microarchitecture is established; (b) and (c) are higher magnification images of the labeled areas shown in (a). The materials shown in (b) and (c) correspond to layers (1) and (2) in Figure 6a. (d) A layer of vertical crystallites (V) precedes the development of the crossed-lamellar structures (CL), just as in wild shell.

TEM using cross-sectional foils has also been used to study the microstructure of the elongated crystals that form between the abnormal tissue and the crossed-lamellar microstructure of regenerated shell. Figure 11a shows a bright-field image of the interface between the enlongated crystals and the crossed-lamellar structure; the inset is a selected-area diffraction pattern from the elongated crystals, after tilting to a zone axis. These electron diffraction patterns confirm the aragonitic nature of the regenerated tissue. The crossed-lamellar structure of regenerated shell further away from this interface looks, for all intents and purposes, identical to the crossed-lamellar structure in wild shell (Figure 11b).

3.3 Microstructure of Conch "Flat Pearls". Tissue regeneration on abiotic substrate—the formation of conch "flat pearls"—shows many similarities to tissue regeneration during wound repair, although mineral formation occurs at shorter time scales during flat pearl formation than during wound repair. However, the time scale of the biomineralization depends on the temperature of the aquarium in which the animals are housed.

These differences can be seen most clearly in XRD patterns. Figure 12a shows a set of experiments conducted in an aquarium maintained at 26 °C. Randomly oriented aragonite is detected 6 h after insertion of a glass cover slip between the mantle tissue and the shell, and a texture that is essentially identical to that found in wild shells appears between 2 and 4 days of tissue formation. The crossed-lamellar microstructure takes much longer to develop during wound repair (Figure 6b).

In some cases, the XRD pattern shows evidence of calcite formation in the first minerals to form. Figure 12b shows XRD data for an experiment conducted in an aquarium maintained at 20 °C; the calcite (10·4) peak, the strongest peak in calcite, is clearly visible at $2\theta = 29.4°$. Although we did not study the effect of temperature on polymorph selection during tissue regeneration in detail, we think that calcite only forms under cooler conditions. (In an early and preliminary report of these experiments,[18] an XRD peak was erroneously labeled as (00·6) calcite. Further study has revealed that this peak is in fact from NaCl due to washing the flat pearl with artificial seawater from the aquarium. The crystals shown in Figure 4a of ref 18 are also NaCl.).

Figure 13a shows a cross-sectional SEM image of a flat pearl grown at 26 °C. The first-formed minerals are aggregates of needlelike crystals. Figure 13b and c show two plan-view images of flat pearls formed at this temperature. Figure 13b shows the "bottom" of the aggregates, i.e., the glass slide side of the flat pearl. Figure 13c shows the mantle side of a flat pearl whose growth was interrupted after 24 h of mineral formation. The extensive matrix present at this stage of tissue regeneration is apparent. Finally, Figure 13d shows the mantle side of a mature flat pearl (cf. Figure 9b).

TEM images of a low-temperature (20 °C) flat pearl grown for short times are shown in Figure 14: (a) is from a calcite region, (b) is from an aragonite region. (These images are from adjacent regions in the same TEM foil.) The aragonite crystallites shown in Figure 14b have developed well-defined crystal faces, which

(18) Su, X.; Heuer, A. H. *Mineralization in Natural and Synthetic Biomaterials*; MRS Proceedings, volume 599, 1999 Fall Meeting.

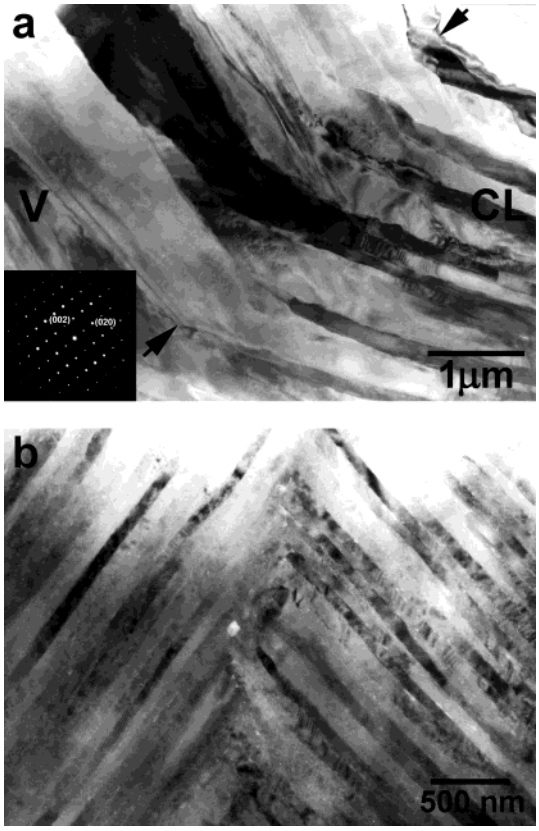

Figure 11. TEM images of regenerated shell tissue: (a) transition from the vertical layer (V) to the crossed-lamellar structure (CL); the dark lamella in the center of the image shows that crystallographic continuity is maintained across the transition region.; (b) side faces of third-order lamellae from two different first-order lamellae in the crossed-lamellar region.

may suggest that soluble organic materials had very little interaction with the growth plane of aragonite under this experimental condition.

Images taken from a cross-sectional flat pearl TEM foil are shown in Figure 15. The microstructure (analogous to region A of Figure 13a) from a region of aggregates of crystallites is shown in Figure 15a; the arrows delineate the boundary of a single aggregate. Figure 15b is from the transition region between the first-formed aggregates of crystallites and crossed-lamellar structures (region B in Figure 13a). Finally, Figure 15c is from the crossed-lamellar structure (region C in Figure 13a); this particular image shows the side faces of third-order lamellae from two different first-order lamellae; the third-order lamellae are nearly horizontal in one first-order lamella (region A) but are nearly vertical in the adjacent first-order lamella (region B).

IV. General Discussion

4.1 Role of the Matrix in Mineralization in the Shell of the Conch, *S. gigas*. As with other biogenic aragonite, the microstructure of the *S. gigas* conch shell differs significantly from any known geological aragonite. The highly ordered organization of lamellae at different hierarchical levels and the uniform scale of the third-order lamellae are compelling evidence that shell formation and growth is a process in which the organic matrix of the shell exerts primary control over mineral deposition.

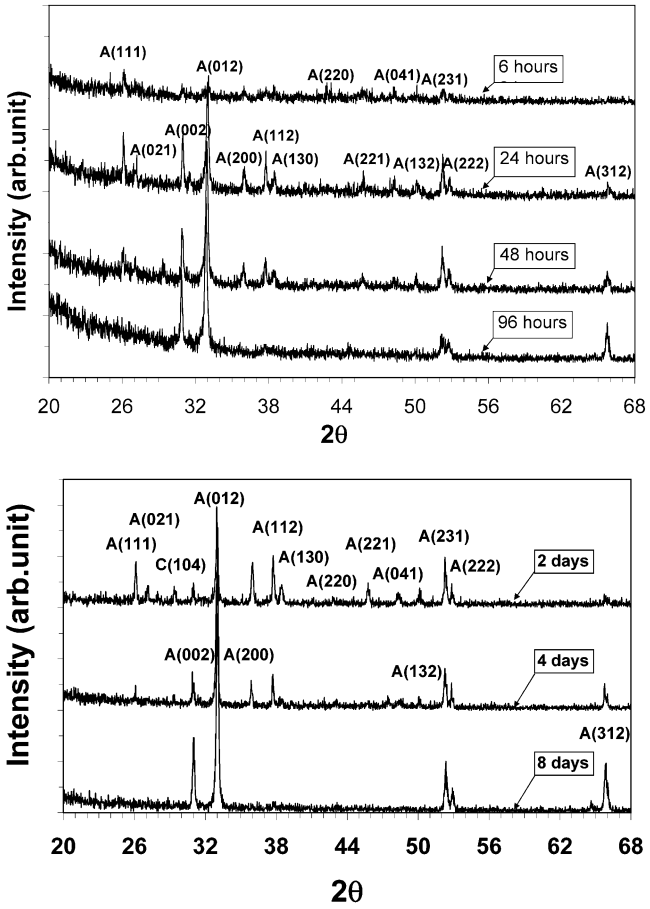

Figure 12. XRD patterns of conch "flat pearls": (a) development of the flat pearls from an animal maintained at 26 °C; (b) similar development for a 20° C experiment. Note that a (10.4) calcite peak (at 29.4° 2θ) only appears in the early stages of the flat pearl development in the cooler aquarium.

The details of how the matrix controls the formation of biogenic aragonite are not understood at a fundamental level in conch shells (nor for that matter in shells which have been studied more extensively, i.e., shells with the nacreous structure). In nacre, a well-defined spatial relationship exists between the aragonite platelets and the underlying organic matrix (chitin and silk fibroin-like protein).[19] The crystallographic **a** and **b** axes of the aragonite platelets are aligned with the long axes of chitin and silk protein macromolecules. The plate-shaped morphology of aragonite in nacre is defined by the preformed, uniformly spaced insoluble protein sheets.[19]

The study of spatial relationship between the organic matrix and aragonite in conch shell is difficult, as the protein content is very small. We have been successful in imaging the organic matrix using partially decalcified specimens. Sheetlike matrix is present at the interfaces between both first-order and second-order lamellae. They are thicker at the latter interfaces and are very thin (<5 nm) at interfaces between third-order lamellae. Though globular features between the large faces of third-order lamellae are the most visible evidence of organic matter, thin organic sheaths connecting the globules completely envelope individual third-order lamella. The globular features are arranged along the

(19) Weiner, S.; Traub, W. *FEBS Lett.* **1980**, *111*, 311.

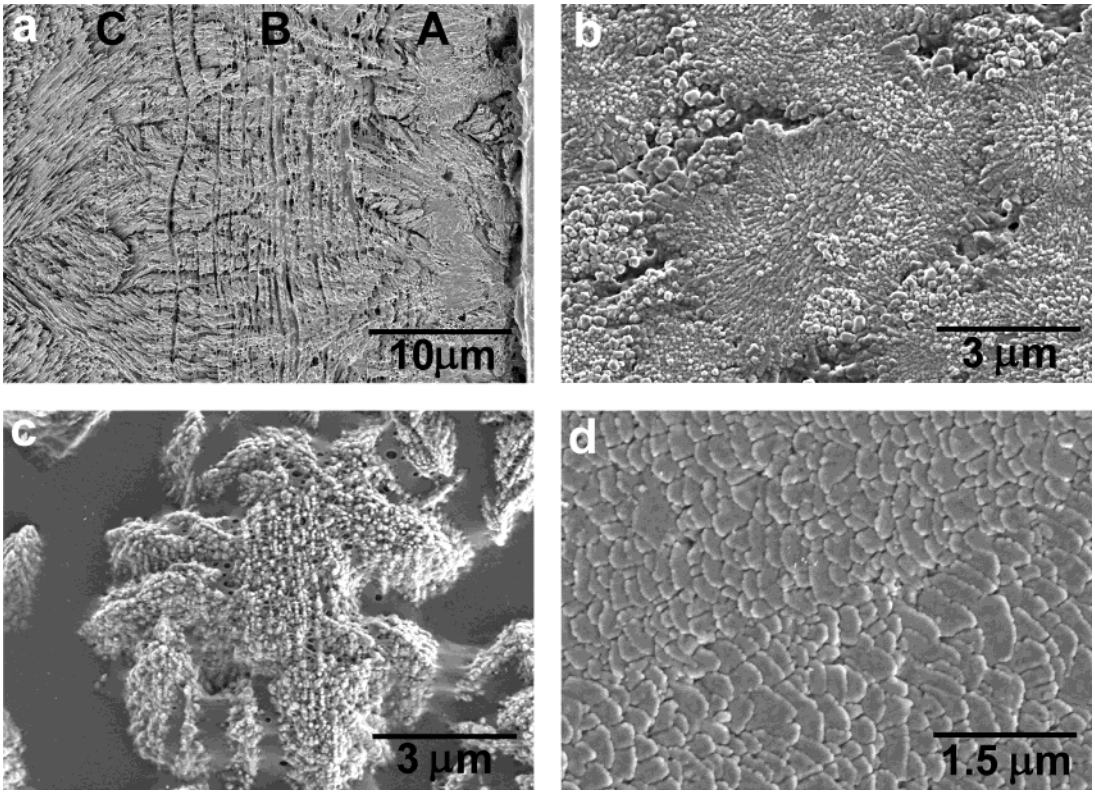

Figure 13. Cross-sectional SEM images of flat pearls grown at 26 °C: (a) ~25 μm of mineral must be formed before the crossed-lamellar microstructure is established; (b) and (c) early-stage microstructures of flat pearls ((b) is an "outside" view while (c) is an "inside" view); (d) a fully developed flat pearl has a structure similar to that of regenerated tissue grown during wound repair (cf. Figure 9a).

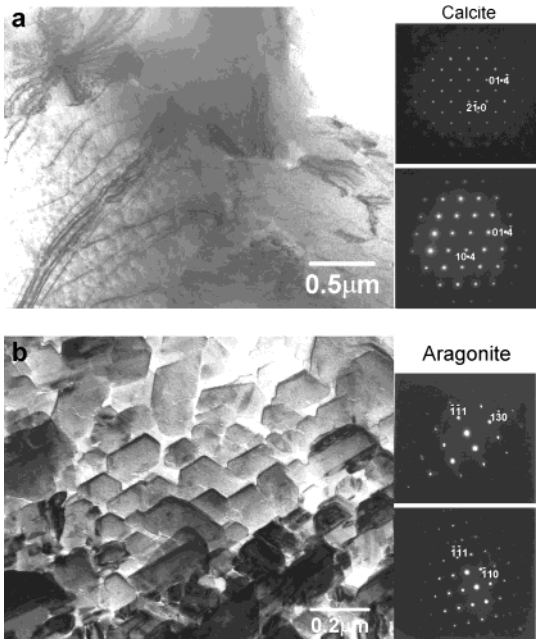

Figure 14. TEM images of a flat pearl grown at 20 °C; these images show minerals formed at early time: (a) calcitic region, (b) aragonite aggregate from the same TEM foil.

top and bottom of each third-order lamella but not along the sides of these lamellae; rather, the matrix between the side faces is very thin and membrane-like.

The presence of organic envelopes around each individual third-order lamellae has been demonstrated by Nakahara et al.[10] In the work of that group, thin sections of the growing edge of the shell parallel to the side faces of the third-order lamellae were studied in juvenile animals. Obliquely oriented envelopes appeared before the deposition of rod-shaped crystals (the third-order lamellae) within the envelopes. These crystals increased in thickness until the organic envelopes contacted one another. This study showed unambiguously that the morphology and orientation of mineral phase is controlled by the preformed organic matrix.

The uniform morphology, dimensions, and ordered organization of third-order lamellae further demonstrate that shell formation in mollusks is a highly controlled process. The modest dimensions of third-order lamellae (~230 nm wide, ~100 nm thick, and several micrometers long) implies the existence of abundant organic matrix around third-order lamellae, whatever the thickness that separates neighboring lamellae. The presence of organic matrix around each third-order lamella and thicker interfaces between first-order and second-order lamellae plays a decisive role in the mechanical properties of the conch shell.[4,14]

4.2 Wound Repair in the Shell of the Conch, *S. gigas*. Conchs are able to repair damage to their shells, as is the case for other mollusks. When damage occurs to conch shells, the animals repair their shells by the mantle tissue covering the damaged areas and secreting the raw materials for repair. Damage in the form of a 4-mm diameter hole can be repaired within 1 to 2 days. The first repaired material consists of layers of organic membranes and aggregates of needlelike crystallites, a morphology which is absent in wild conch shell.

No periostracum was observed in the process of shell repair. Thus, the initial shell repair process is different from normal shell growth in which periostracum is

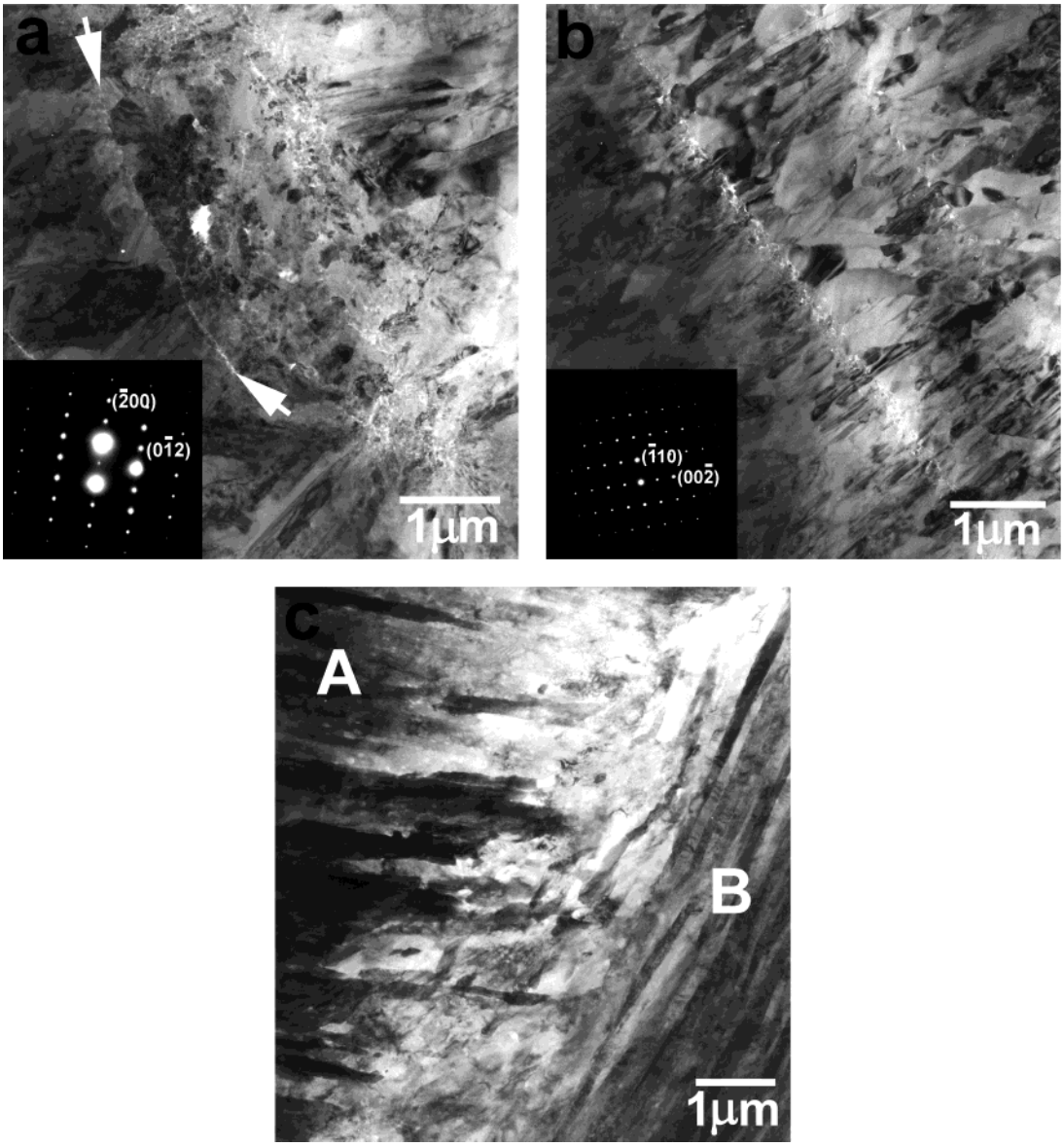

Figure 15. Cross-sectional TEM images from a flat pearl grown at 26 °C: (a) an aragonite aggregate, whose boundary is shown by an arrow; (b) the transition region between the first formed aragonite and the fully developed crossed-lamellar structure shown in (c).

secreted first and acts as a substrate for the crossed-lamellar deposit.

Nonperiostracum-type organic membranes have also been observed in other mollusks. In *Helix pomatia*, homogeneous sheets or reticulate fibers of organic matrix have been observed.[12,13] In the prismatic and nacreous layers of the shells of some bivalves, deposition of collagen fibrils has also been reported.[20]

We also observed collagen fibers at the beginning of shell regeneration in the "lidless" wound repair. On the basis of the experimental results of Abolinš-Krogis and Smina et al., amoebocytes should be involved in the synthesis of collagen.[21,22] It may be that lidless wound repair triggers the appearance of amoebocytes in the damaged area of the shell and thus leads to the secretion of collagen as a scaffold for shell repair.

It seems that periostracum-type organic membrane can be formed only when the epithelium of the mantle edge is involved with the shell repair process.[11] In cases when periostracum is produced, normal shell is developed in the repair process.[11]

Initial mineralization of the first-formed organic membranes in conchs involves aggregates of needlelike aragonite; this is quite different from mineralization of the periostracum in wild animals. As the number of the aggregates increase, they form a continuous layer which does not have its counterpart in normally developing shell. Rather, this structure must be a pathological deposition product to protect the shell until the crossed-lamellar inner part of the shell can develop.

Although the aggregates of needlelike crystallites formed during wound repair are an abnormal form of aragonite in conch shells, it is the same polymorph as the $CaCO_3$ in wild shell. Similar aggregates also formed during flat pearl formation at 26 °C. However, a small amount of calcite was detected in the first-deposited

(20) Travis, D. *Ultrastruct. Res.* **1967**, *18*, 519.
(21) Abolinš-Krogis, A. *Cell Tiss. Res.* **1976**, *172*, 455.
(22) Sminia, T.; Pietersma, K.; Scheerboom, J. E. M. *Z. Zellforsch. Mikrosk. Anat.* **1973**, *141*, 561.

mineral in "flat pearls" grown at 20 °C. It seems that higher temperature is favorable for conch to produce aragonite in the process of tissue regeneration. Such an effect has also been demonstrated in shell regeneration in snails, *Viviparus intertextus*.[24] The general effect of increasing temperature within the range of 13 to 25 °C in this species was to bring an increase in the percentage of aragonite and a decrease in the percentage of calcite and vaterite.

Several other factors may also affect the crystals produced during shell repair, including the chemical and structural characteristics of the organic matrix within mollusk shell. The effect of organic matrix on the polymorph of crystals has been investigated by both in vivo[23−25] and in vitro experiment,[26,27] with the effect being more clear in in vitro experimental systems. In such studies, mineral-specific proteins extracted from either aragonitic or calcitic shell were added to aqueous solutions in which $CaCO_3$ was crystallizing. The mineral-specific soluble proteins controlled the polymorph of mineral formed in such crystallization experiments with high fidelity.[26,27]

V. Conclusions

We have studied the microstructures of wild shells and of regenerated tissue in *S. gigas*. Differences do exist between normal shell growth and shell regeneration. In conch shell repair, the nature of the first-formed organic matrix is altered and differs from the mineralization of periostracum found in wild shell. Consequently, the first-formed minerals associated with such organic matrix have an abnormal morphology. Such differences occur only at the beginning of shell repair; during the later stages of repair, a crossed-lamellar structure is developed which has a structure essentially identical to that present in wild conch shell.

Acknowledgment. This work was supported by EPRI. We thank Dr. Robert Glazer of the Caribbean Marine Research Institute for providing us with juvenile conchs. The optical micrograph in Figure 2b was taken by Dr. V. J. Laraia.

CM030573L

(23) Watabe, N.; Wilbur, K. M. *Nature* **1960**, *188*, 334.
(24) Wilbur, K. M.; Watabe, N. *Ann. N. Y. Acad. Sci.* **1963**, *109*, 82.
(25) Fritz, M.; Belcher, A. M.; Radmacher, M.; Walters, D. A.; Hansma, P. K.; Stucky, G. D.; Morse, D. E.; Mann, S. *Nature* **1994**, *371*, 49.
(26) Falini, G.; Albeck, S.; Weiner, S.; Addadi, L. *Science* **1996**, *271*, 67.
(27) Belcher, A. M.; Wu, X. H.; Christensen, R. J.; Hansma, P. K.; Stucky, G. D.; Morse, D. E. *Nature* **1996**, *381*, 56.